Research on Catalytic Denitrification by Zero-Valent Iron (Fe0) and Pd-Ag Catalyst

Yu Zhou
Hebei GEO University

Yupan Yun (✉ yundzdx@126.com)
Hebei GEO University

Xueyou Wen
Hebei GEO University

Research Article

Research on catalytic denitrification by zero-valent iron (Fe^0) and Pd-Ag catalyst

Yu Zhou[1], Yupan Yun[1]*, Xueyou Wen[1]*

1 School of Water Resources and Environment, Institute of Intelligence and Environment industry Technology, Hebei Province Collaborative Innovation Center for Sustainable Utilization of Water Resources and Optimization of Industrial Structure, Hebei Province Key Laboratory of Sustained Utilization and Development of Water Resources, Hebei GEO University, 050031, Shijiazhuang, Hebei, China

* Corresponding author: Yupan Yun, E-mail: yundzdx@126.com; Xueyou Wen, E-mail: 469890836@qq.com Tel: +86-0311-87208362

Abstract: This study primarily focused on how to effectively remove nitrate by catalytic denitrification through zero-valent iron (Fe^0) and Pd-Ag catalyst. In order to get better catalytic performance, response surface methodology (RSM), instead of the single factor experiments and orthogonal tests, was firstly applied to optimize the condition parameters of the catalytic process. Results indicated that RSM is accurate and feasible for the condition optimization of catalytic denitrification. Better catalytic performance (71.6% N$_2$ Selectivity) was obtained under the following conditions: 5.1 pH, 127 min reaction time, 3.2 mass ration (Pd: Ag), and 4.2 g/L Fe^0, which was higher than the previous study designed by the single factor experiments (68.1%) and orthogonal tests (68.7%). However, under the optimal conditions, N$_2$ selectivity showed a mild decrease (69.3%), when the real wastewater was used as the influent. Further study revealed that the cations (e.g., K$^+$, Na$^+$, Ca^{2+}, Mg^{2+}, and Al^{3+}) and anions (e.g., Cl$^-$, HCO$_3^-$, and SO$_4^{2-}$) exist in wastewater may have distinctive influence on N$_2$ selectivity. Finally, the reaction mechanism and kinetic model of catalytic denitrification were further studied.

Keyword: Nitrate removal; Catalytic denitrification; Response surface methodology (RSM)

Declarations

(1) Funding

(2) Competing interests

The authors declare that they have no competing interests.

(3) Authors' contributions

Yu Zhou conducted the experiments and wrote the manuscript. Yupan Yun and Xueyou Wen helped do the experiments and revised the manuscript. All authors read and approved the final manuscript.

(4) Availability of data and materials

The datasets used and/or analyzed during the current study are available from the corresponding author on reasonable request.

(5) Ethics approval and consent to participate

Not applicable

(6) Consent for publication

Not applicable

1. Introduction

Contamination with nitrate (NO_3^-) in water resource has attracted increasing public concern. Nitrate detected in surface water and groundwater is a common contaminant that can cause severe health risks, such as blue baby syndrome, cancer, as well as the eutrophication of water bodies (Jasper et al. 2014) According to the research, agricultural activities (mainly the over-fertilization of nitrogenous fertilizers), atmospheric deposition, sewage discharges, and the spreading of sewage sludge and manure to land all contribute to nitrate pollution (Khalil et al. 2016).

Several technologies have been developed for the treatment of nitrate-contaminated water. In general, these include physico-chemical denitrification (such as ion exchange, reverse osmosis, chemical precipitation, and electrocoagulation), biological treatment, and chemical reduction (Min et al. 2013). Among these approaches, biological denitrification, and catalytic hydrogenation proved to be the most promising technologies that could selectively reduce nitrate to nontoxic nitrogen (N_2) (Mcadam and Judd 2006; Jung et al. 2014). However, the biological method requires intensive maintenance and constant addition of carbon resources to the system. Additional drawbacks include excessive biomasses disposal and treatment (aeration and disinfection) of denitrified water. Moreover, these microbial approaches are generally slow and sometimes incomplete compared to chemical reduction (Soares 2000). In recent years, the technology of chemical catalytic reduction of nitrate attracts more attention.

In 1989, Vorlop and Tacke first put forward the traditional chemical catalytic hydrogenation that utilized the reductant H_2 and bimetal catalyst for nitrate reduction (Vorlop and Tacke, 1989). In this catalytic process, catalyst plays the indispensable role, while H_2 has been regarded as the reductant, which could provide the needed H obtained through catalytic reaction to participate in the deoxidation process of the nitrate reduction. However, the major problem of this technology that we

cannot ignore is the low solubility of H_2 in aqueous media and the operational complexity (appropriate H_2 flow rate, and pressure). Several researchers replaced H_2 with an organic acid (e.g., HCOOH) or its salt (e.g., NaCOOH) involved in nitrate removal and formation of N_2 through the deoxidization reaction with nitrate (Choi et al. 2013). However, the incomplete decomposition of acid or its salt and the threat to human health greatly restricts its wide application. Based on these studies, great efforts were made to try and solve these issues and the novel synergistic effect of zero-valent iron (Fe^0) reductant and bimetallic catalyst for nitrate reduction was proposed.

The experimental design for evaluating and optimizing experimental parameters makes it possible to minimize costs and maximize desired responses (Ye et al. 2016; Nathany et al, 2014). For most researchers, the single factor experiments and orthogonal tests have been widely used for the experimental design and analyses. However, these two methods are incapable of getting the true optimal conditions due to ignoring the interactions among influential variables (Shen et al. 2016). Therefore, instead of these two methods, Response Surface Methodology (RSM) was utilized for modeling and optimizing the catalytic denitrification conditions in this paper. RSM is a particular set of mathematical and statistical approaches developed for the design of experiments building models, evaluating the effects of variables, and determining the optimum conditions of the variables (Haddar et al. 2014). This method contributes to completing the comprehensive design with a minimum number of experiments, analyzing the interaction between the parameters, and more directly and accurately obtaining the optimal operation parameters (Imran and Awais, 2016).

Actually, until now, RSM has not been used as a modeling and optimization tool for catalytic reduction of nitrate. Hence, in this research, Box-Behnken Design (BBC) of Response Surface Methodology (RSM) was used as a design framework to model and optimize the processes of catalytic denitrification by zero-valent iron (Fe^0) and Pd-Ag catalyst. The individual and interactive effects of the key process variables such as pH, reaction time, Pd:Ag mass ratio, and Fe^0 dosage was were evaluated and mathematically modeled. Furthermore, the reaction mechanism of the catalytic denitrification was comprehensively illustrated.

2. Material and methods

2.1 Materials

The chemical reagents used in this research were: sodium nitrate ($NaNO_3$), silver nitrate ($AgNO_3$), palladium chloride ($PdCl_2$), hydrochloric acid (HCl), iron powder (<0.07 nm, >98 %), graphene, SiO_2, diatomite, kaolin, γ-Al_2O_3, and silica gel. The catalyst (e.g. Pd-Ag/graphene) can be

obtained through the traditional wet impregnation method (Yun et al, 2016). All chemical reagents were of analytical grade.

2.2 Experimental design

Batch experiments were completed to investigate the potential factors that may impact catalytic performance. All tests were performed in a 1 L plexiglas reactor (see Fig. 1). 20 mg/L of synthetic solution ($NaNO_3$) was continuously pumped into the reactor to do the RSM analysis and get the optimal catalytic conditions. Then, the real wastewater obtained from a wastewater treatment plant was utilized as the influent. The effect of cations and anions may exist in wastewater on catalytic denitrification was further investigated. Certain amounts of Fe^0 and 4 g/L catalyst were added to the reactor prior to the experiments. To guarantee a better mass transfer effect in the system, the reactor was placed on an magnetic stirrer under 450 rpm at room temperature (20±5 °C). Simultaneously, 1 mol/L HCl was added to the system by a ZDJ-5 automatic titrator to remain the same level of solution pH during the whole process.
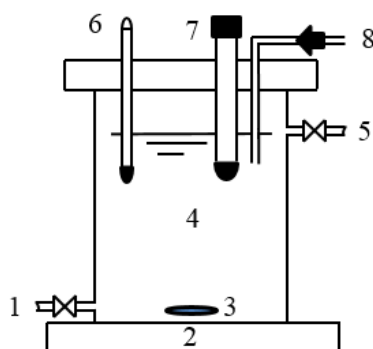

Fig. 1 Schematic of the reactor

1: influent; 2: magnetic stirrer; 3: rotor; 4: reactor; 5; effluent; 6: thermometer; 7: pH meter; 8: automatic titrator

Samples were periodically collected to determine the concentration of nitrate-nitrogen (NO_3^--N), nitrite-nitrogen (NO_2^--N), ammonium (NH_4^+-N) and total nitrogen (TN) after 0.45 μm membrane filtration. NO_3^-, NO_2^- and TN were measured with an ion chromatograph (DIONEX-120), while NH_4^+ was tested via the Nessler's reagent spectrophotometry.

The N_2 selectivity was calculated as:

$$N_2 \text{ selectivity } (\%) = \frac{C_{N_2}}{C_0 - C_t} \times 100\% \qquad (1)$$

Where C_0 is the initial nitrate concentration (mg/L), C_t is the nitrate concentration (mg/L) at time t (min), C_{N_2} is the content of N2 (mg/L), which was calculated via quantity balance, assuming that the NOx produced is negligible.

3. Results

3.1 RSM analysis

(1) Box-Behnken design (BBD)

Table 1 Levels of Box-Behnken design

Factor	Levels		
	-1	0	+1
pH(X_1)	4.1	5.1	6.1
Time/min ((X_2)	90	120	150
Pd:Ag mass ratio(X_3)	2:1	3:1	4:1
Fe^0 dosage/g/L(X_4)	3	4	5

Table 2 Box-Behnken design and results

Number	X_1	X_2/min	X_3	X_4/g/L	N2 selectivity/%
1	-1	0	0	1	55
2	-1	0	1	0	56
3	0	-1	1	0	64
4	0	1	-1	0	65
5	0	-1	-1	0	60
6	1	1	0	0	59
7	0	-1	0	1	64
8	-1	0	0	-1	53
9	0	1	1	0	68

10	0	1	0	-1	64
11	0	0	0	0	68
12	0	0	0	0	69
13	1	0	-1	0	58
14	0	1	0	1	66
15	-1	-1	0	0	56
16	0	0	1	-1	65
17	-1	0	-1	0	55
18	0	0	1	1	70
19	1	-1	0	0	56
20	0	-1	0	-1	62
21	0	0	0	0	69
22	0	0	-1	1	65
23	1	0	0	1	61
24	-1	1	0	0	57
25	0	0	-1	-1	60
26	1	0	1	0	61
27	1	0	0	-1	65

(2) Regression equation fitting and analysis of variance (ANOVA)

The software of Minitab 17 was applied to the multiple regression fitting. Based on the data in Table 2, the quadratic multinomial regression equation was listed as follows, and the regression equation coefficients and T test can be seen in Table 3:

Y (N_2 selectivity) = 69.67 + 0.583 X_1 + 1.000 X_2 + 1.833 X_3 + 1.750 X_4 - 17.708 X_1*X_1 - 2.833 X_2*X_2 - 2.833 X_3*X_3 - 1.958 X_4*X_4 + 2.500 X_1*X_2 + 1.000 X_1*X_3 - 1.250 X_1*X_4 + 0.750 X_2*X_3 + 1.250 X_2*X_4+ 0.250 X_3*X_4

Table 3 Regression equation coefficients and T test

Term	Coefficient	Standard error coefficient	T-Value	P-Value
Constant	69.67	1.12	62.14	0.000
X_1	0.583	0.561	1.04	0.019
X_2	1.000	0.561	1.78	0.100
X_3	1.833	0.561	3.27	0.007
X_4	1.750	0.561	3.12	0.009
$X_1 X_1$	-17.708	0.841	-21.06	0.000
$X_1 X_2$	-2.500	0.971	-2.57	0.024
$X_1 X_3$	0.500	1.14	0.44	0.670
$X_1 X_4$	-1.250	0.971	-1.29	0.222
$X_2 X_2$	-2.833	0.841	-3.37	0.006
$X_2 X_3$	0.750	0.971	0.77	0.455
$X_2 X_4$	1.250	0.971	1.29	0.222
$X_3 X_3$	-2.833	0.841	-3.37	0.006
$X_3 X_4$	0.250	0.971	0.26	0.801
$X_4 X_4$	-1.958	0.841	-2.33	0.038

Note: $P < 0.05$, significant level; $P > 0.05$, below significant level (Yu et al, 2018)

As depicted in Table 3, the linear term- X_1, X_3 and X_4, the interaction terms- X_1X_2, X_1X_4, and all the square terms- X_1X_1, X_2X_2, X_3X_3 X_4X_4 remarkably affect the test results ($P < 0.05$). Whereas, X_1, X_2, X_1X_3, X_1X_4, X_2X_3, X_2X_4, X_3X_4 have no significant impact on the experimental results.

Table 4 Analysis of variance (ANOVA) results of the quadratic experimental model

Source	DF	Adj SS	Adj MSS	F-Value	P-Value
Model	14	596.935	42.638	8.13	0.000
Linear	4	138.167	34.542	6.59	0.005
X_1	1	65.333	65.333	12.46	0.004

X_2	1	24.083	24.083	4.59	0.053
X_3	1	36.750	36.750	7.01	0.021
X_4	1	12.000	12.000	2.29	0.156
Square	4	447.519	111.880	21.34	0.000
$X_1 X_1$	1	436.009	436.009	83.16	0.000
$X_2 X_2$	1	45.370	45.370	8.65	0.012
$X_3 X_3$	1	25.037	25.037	4.78	0.049
$X_4 X_4$	1	17.120	17.120	3.27	0.096
2-way interaction	6	11.250	1.875	0.36	0.892
$X_1 X_2$	1	1.000	1.000	0.19	0.670
$X_1 X_3$	1	1.000	1.000	0.19	0.670
$X_1 X_4$	1	9.000	9.000	1.72	0.215
$X_2 X_3$	1	0.250	0.250	0.05	0.831
$X_2 X_4$	1	0.000	0.000	0.00	1.000
$X_3 X_4$	1	0.000	0.000	0.00	1.000
Error	12	62.917	5.243		
Total	26	659.852			
Lack-of-Fit	10	60.917	6.092	6.09	0.149
Pure error	2	2.000	1.000		

$R^2 = 90.47\%$

As exhibited in Table 4, P-value= 0.000 <0.01, and R^2=90.47, which prove the model built in this paper accurately and significantly (Kabdasli and Coskun, 2015). Additionally, the regression equation obtained has been better fitted. Therefore, it comes to the conclusion that this model mentioned above can be used to continuously analyze and predict the experimental data.
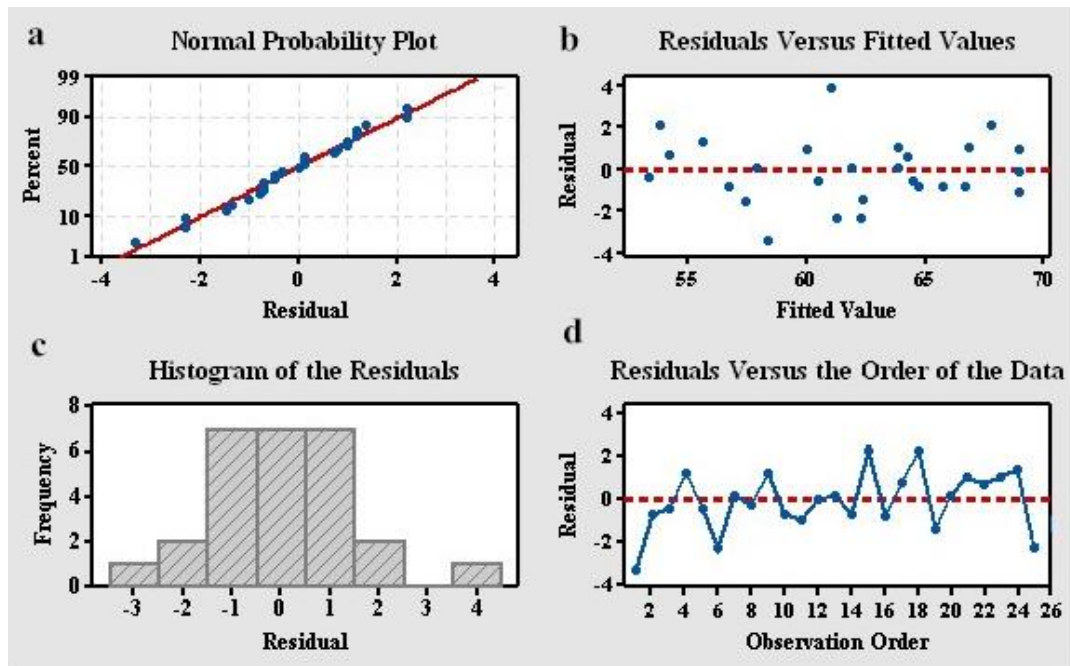
Fig. 2 Residual plots for N_2 selectivity

In addition, in the ordinary least squares (OLS) regression analysis, in order to validate the model you proposed, the residual plots should be checked, which were listed in Fig. 5. It's believed that randomness and unpredictability are essential components for any valid regression model. Through the residual plots analyses, whether the observed error (residuals) is consistent with stochastic error can be accurately assessed. The residuals should be centered on zero throughout the range of fitted values indicated in Fig. 2b and 2d. On the other hand, random errors assumed to produce residuals should be normally distributed. In other words, the residuals should fall in a symmetrical pattern and have a constant spread throughout the range which can be proved in Fig. 2a and 2c.

(3) 3D response surface analyses
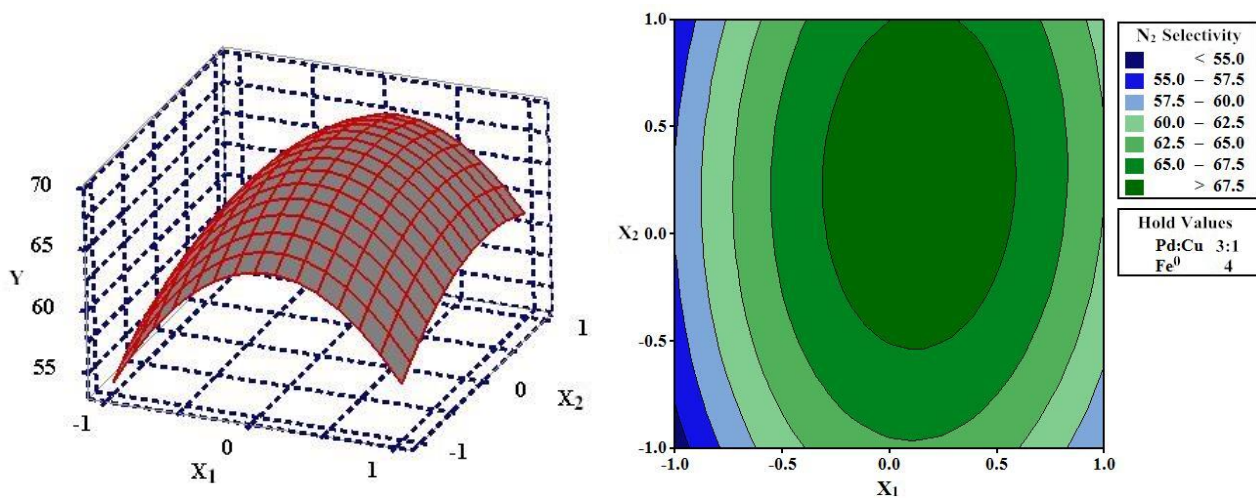
a Response surface (Left) and Contour plots (Right) of X_1 and X_2 on N_2 selectivity
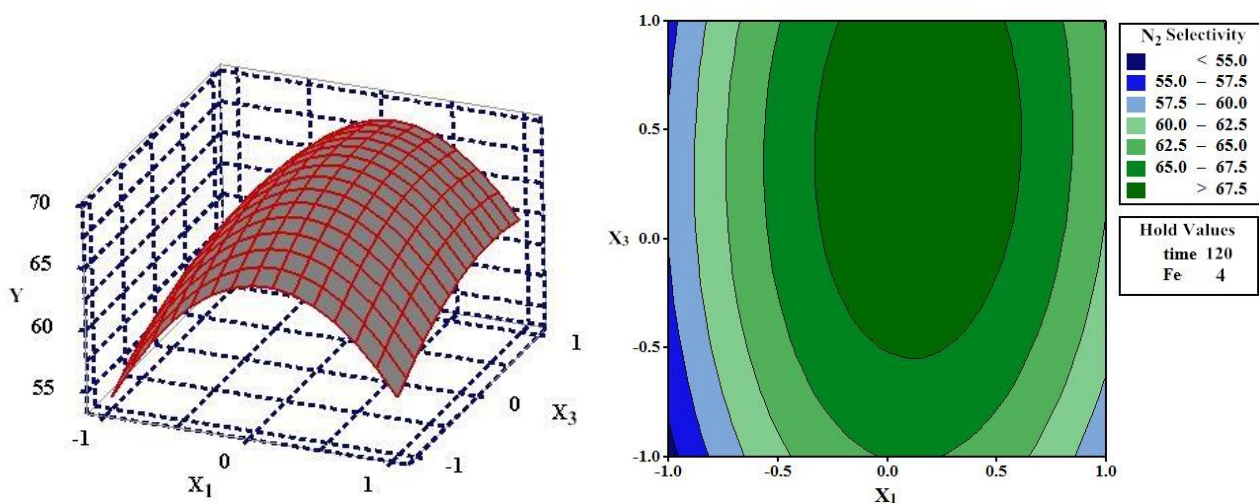
b Response surface (Left) and Contour plots (Right) of X_1 and X_3 on N_2 selectivity
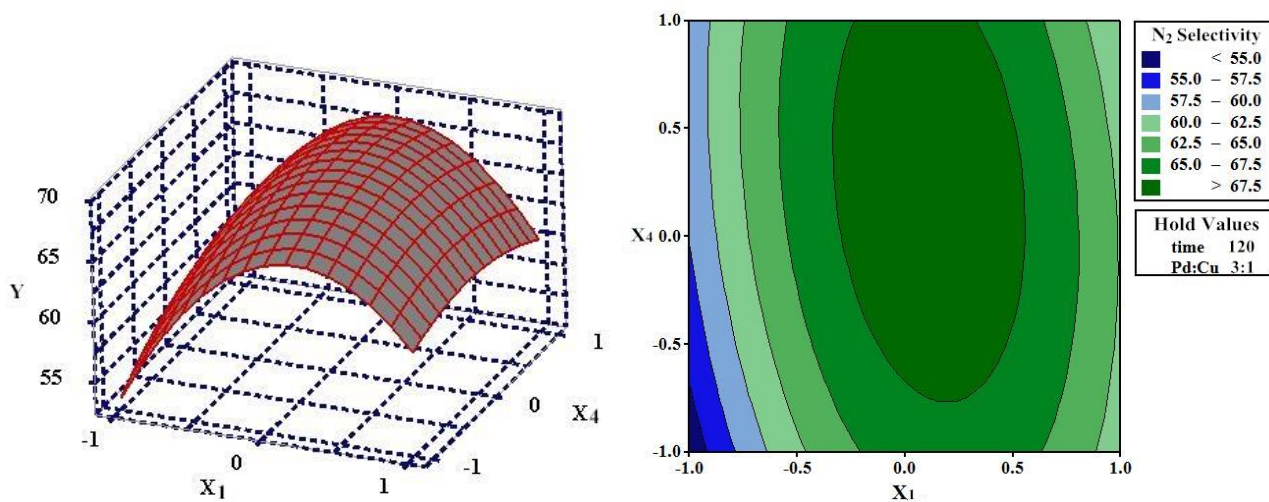
c Response surface (Left) and Contour plots (Right) of X_1 and X_4 on N_2 selectivity
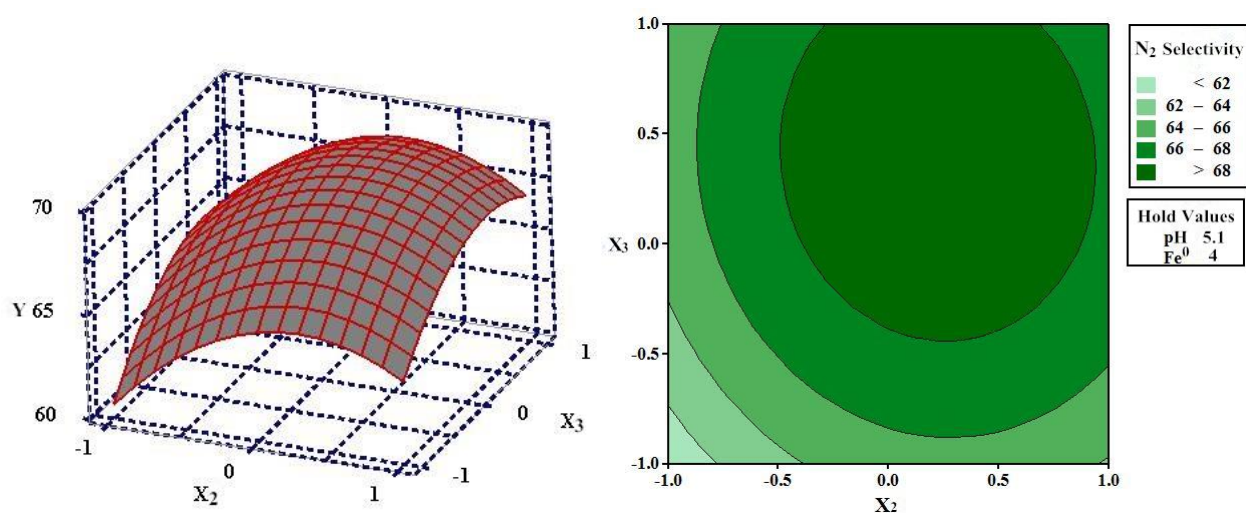
d Response surface (Left) and Contour plots (Right) of X_2 and X_3 on N_2 selectivity
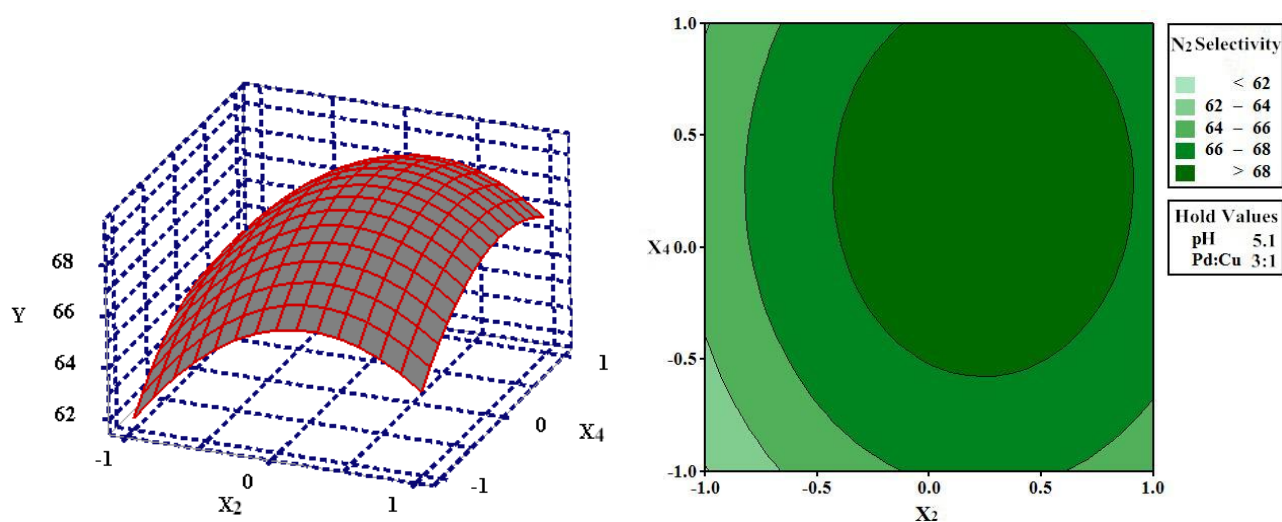
e Response surface (Left) and Contour plots (Right) of X_2 and X_4 on N_2 selectivity
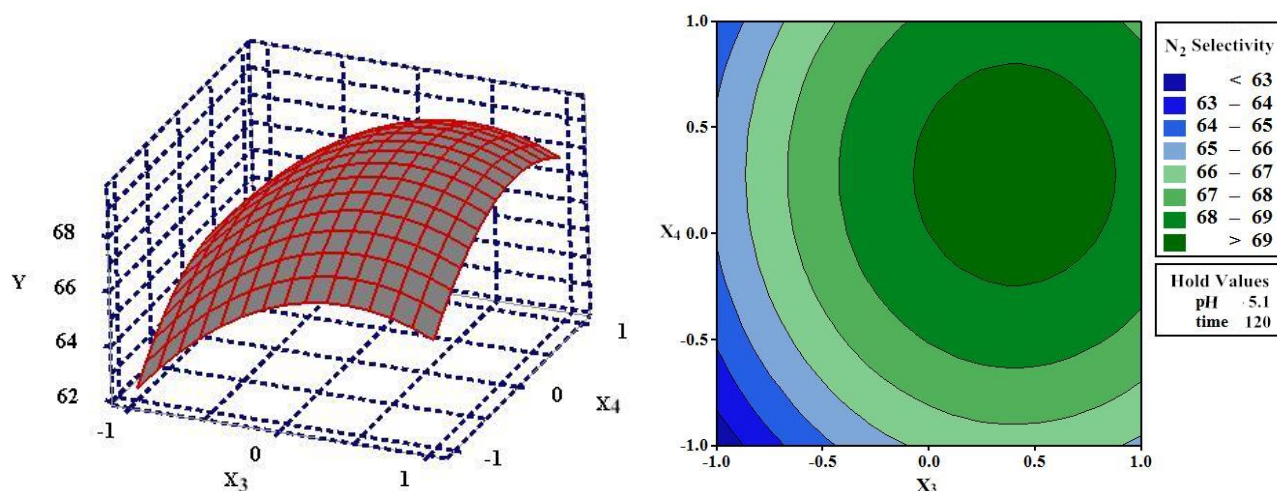
f Response surface (Left) and Contour plots (Right) of X_3 and X_4 on N_2 selectivity

Fig. 3 Response surface and Contour plots between two factors

3D response surface analyses were further conducted for the four factors, including pH, time, Pd:Ag mass ratio, and Fe^0 dosage, which can be seen in Fig. 3. Response surface and contour plots have been applied to intuitively indicate the influence of various factors on the responses, so as to find out the optimal process parameters and the interaction between the parameters (Dadras et al. 2014). In the contour plots, the central point of the minimum ellipse is the highest point of the response surface. Additionally, the shape of the contour line can reflect the strength of the interaction, and the oval indicates that the interaction between the two factors is significant, while the circle reflects the opposite meaning.

As depicted in Fig. 3a, compare with others, response surface and contour plots of X_1 and X_2 on N_2 selectivity show the significant influence trend, which is consistent with the data in Table 3. In order to obtain the predicted maximum value through the model we build, the canonical analysis of response surface was conducted, which was listed in Table 5.

Table 5 Canonical analysis of response surface

Factor	X_1	X_2	X_3	X_4	Type of stable point
Coded value	0.13	0.23	0.41	0.23	maximum value
Actual value	5.1	127	3.2	4.2	69.8%

As indicated in Table 5, the predicted maximum value is 69.8%. The actual values of the four factors (X_1, X_2, X_3, and X_4) got from the coded value are: 5.1 pH, 127 min time, 3.2 Pd: Ag, and 4.2 g/L Fe^0, respectively, which are the predicted optimal parameters.

(4) Validation test

Based on the predicted optimal parameters in Table 5, the validation experiments were conducted under the following conditions: 5.1 pH, 127 min reaction time, 3.2 mass ration (Pd: Ag), and 4.2 g/L Fe^0. Results showed that the N_2 selectivity of the catalytic denitrification reached 71.6%, higher than the study designed by the single factor experiments (68.1%) and orthogonal test (68.7%) in Table 6, which proves that the model used in this research is accurate and can get the true optimal conditions for the catalytic reduction of nitrate.

Table 6 N_2 selectivity with different designs

Design method	pH	Time (min)	Pd:Ag mass ratio	Fe^0 dosage (g/L)	N_2 selectivity (%)
Single-factor design	5.2	120	3:1	4	68.1
Orthogonal test	4.2	120	3:1	5	68.7
RSM design	5.1	127	3.2:1	4.2	71.6

3.2 Simulation experiments of real wastewater

To test the effect of water quality on N_2 selectivity, real wastewater obtained from the secondary effluent of a municipal wastewater treatment plant in Beijing, China, was adopted for batch experiments. The properties of water samples were: concentration of NO_3^-- N: 19.2 mg/L, NO_2^-- N: 0.1 mg/L, NH_4^+- N: 0.2 mg/L, TN: 21 mg/L, and pH: 6.7. The catalytic conditions were: 5.1 pH, 127 min reaction time, 4 g/L catalyst: Pd-Ag/graphene, Pd:Ag =3.2:1, Pd: 5 wt%, and 4.2 g/L Fe^0.

As described in Table 7, compared to the artificial solution ($NaNO_3$) as influent, N_2 selectivity showed a mild decrease as the real wastewater was used as the influent. This phenomenon may be due to the ions that exist in the wastewater. Therefore, the effect of the ions on catalytic performance was further investigated.

Table 7 Water quality analyses of the effluent

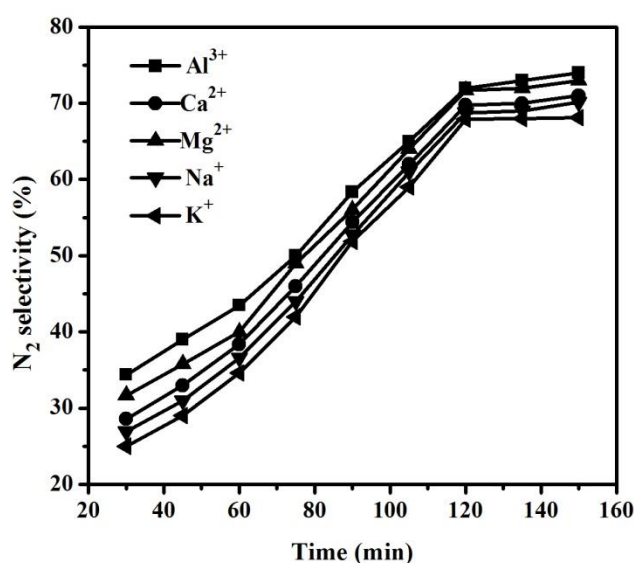| Water sample	pH	NO_3^--N (mg/L)	NH_4^+-N (mg/L)	NO_2^--N (mg/L)	TN (mg/L)	N_2 selectivity (%)
Wastewater	8.4	10.2	3.3	0.2	14.7	69.3
NaNO$_3$	8.2	8.9	3.4	0.1	13.6	71.6

Fig. 4 Catalytic performances with different cations in solution

(pH 5.1, 127 min, 4.2 g/L Fe^0, 4 g/L Pd-Ag/graphene, Pd:Ag=3:1, Pd: 5 wt%)

Fig. 4 shows the effect of different cations on N_2 selectivity for nitrate reduction. 20 mg/L of artificial solutions (Al(NO$_3$)$_3$, Ca(NO$_3$)$_2$, Mg(NO$_3$)$_2$, KNO$_3$, NaNO$_3$) were respectively prepared prior to the experiments.

A series of experiments using various nitrate salts as a source of nitrate ions revealed that the catalytic performance increased in the order: $K^+ < Na^+ < Ca^{2+} < Mg^{2+} < Al^{3+}$. It has been reported that these cations have different influence on the migration rate of NO$_3^-$ and OH$^-$ in the water body (Cui et al. 2008). Cations with high valence or small radius seem more likely to have a strong ability to bond with NO$_3$-, preventing NO$_3^-$ from catalytic reduction. Similarly, the cations in solution tend to strongly adsorb the formed OH$^-$ that may have a negative impact on catalytic denitrification, enhancing the separation of OH$^-$ from bimetal active sites on the surface of the catalyst and offering suitable space and conditions for a catalytic reaction (Zhang, 2003).
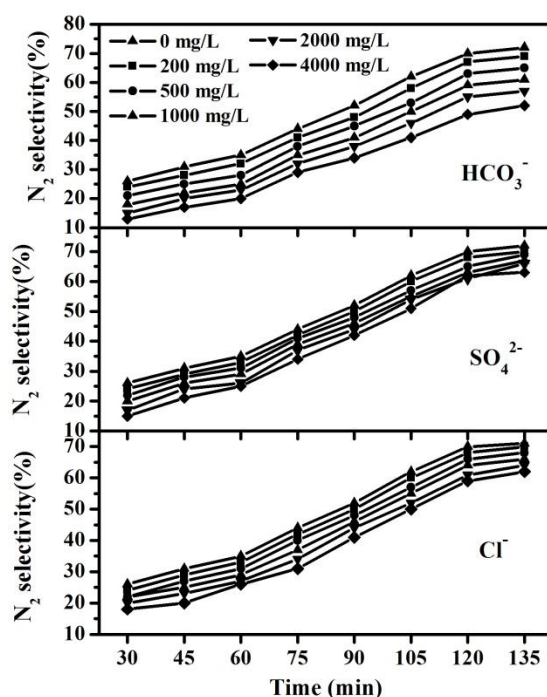
Fig. 5 catalytic performances with different anions in solution

(pH 5.1, 127 min, 4.2 g/L Fe^0, 4 g/L Pd-Ag/graphene, Pd:Ag=3:1, Pd: 5 wt%)

As depicted in Fig. 5, the impact on N$_2$ selectivity with Cl$^-$, SO$_4^{2-}$, and HCO$_3^-$ were respectively investigated. It was apparent that HCO$_3^-$ partially contributed to the decrease of catalytic efficiency. The higher the HCO$_3^-$ concentration, the more obvious the resulting catalytic effects were. This result was mainly derived from the fact that HCO$_3^-$ possesses a similar plane structure than NO$_3^-$, which leads to adverse influence on nitrate reduction, as a result of the competitive adsorption with NO$_3^-$ on the surface of the catalyst (Zhang, 2003). In contrast, due to the different structure, Cl$^-$ and SO$_4^{2-}$ both had little to do with catalytic nitrate reduction (Deganello et al, 2000).

3.3 Reaction mechanism

(1) Role of the reductant-Fe^0

In the catalytic process, Fe^0 primarily served as electron donor. In general, the removal of nitrate by Fe^0 involved the directional electron transfer from Fe^0 to nitrate, which is then converted into non-toxic N$_2$ or less toxic species (NO$_2^-$ and NH$_4^+$) (Ryu et al. 2011). In practical terms, at the metal active sites that are located at the surface of the carrier, the electron that Fe^0 lost could bond with H$^+$ in solution and form active H, which took part in the deoxidization process and reduced NO$_3^-$, as shown in Fig. 6.
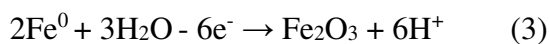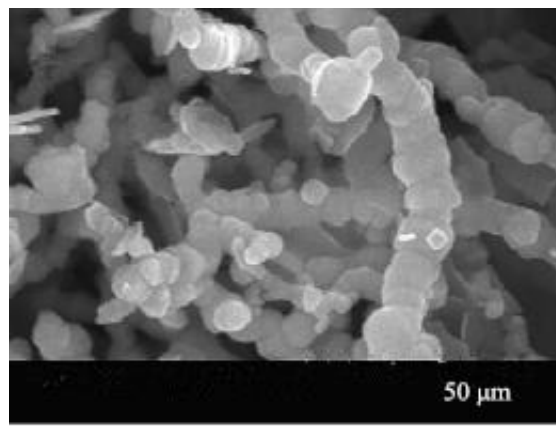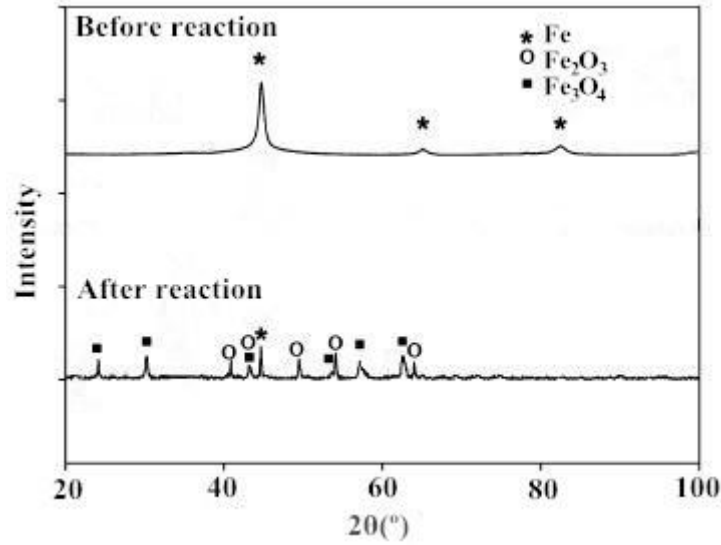
15
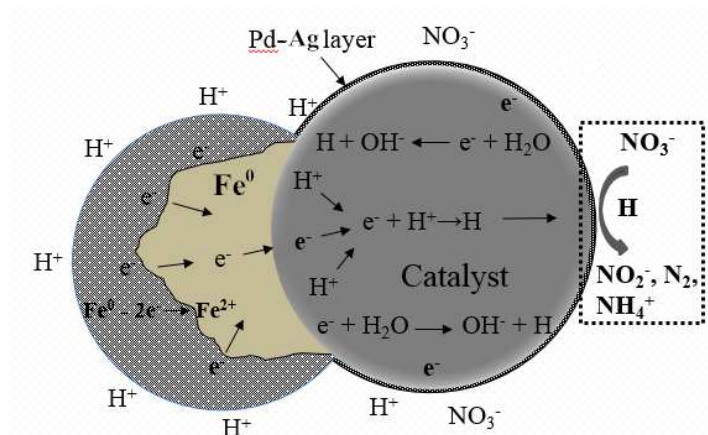
Fig. 6 Role of Fe^0 in catalytic process

SEM images and XRD patterns of Fe^0 before and after catalytic process were shown in Fig. 7. According to Fig. 6a and 6b, it's obvious to find that the morphology of the surface of Fe^0 changed after catalytic reaction. Magnetite (Fe_3O_4) and hematite (Fe_2O_3) were detected on the surface of Fe^0 through the XRD analysis, which is consistent with the Schlicker's finding (Schlicker et al. 2000). The possible reaction equations are listed as below:

$$Fe^0 - 2e^- \rightarrow Fe^{2+} \qquad (2)$$

$$2Fe^0 + 3H_2O - 6e^- \rightarrow Fe_2O_3 + 6H^+ \qquad (3)$$

$$3Fe^0 + 4H_2O - 8e^- \rightarrow Fe_3O_4 + 8H^+ \qquad (4)$$
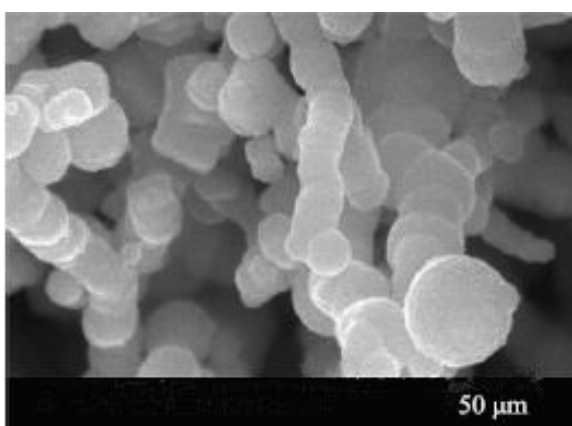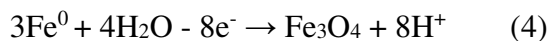
a

b

c

Fig. 7 SEM images and XRD patterns of Fe^0

a：SEM image before reaction；b：SEM image after reaction；c：XRD patterns

(2) Catalytic denitrification process

It's believed that the catalytic reduction of nitrate has been achieved with the stepwise processes. As indicated in the equations (Eq. 5-11) (Hao and Zhang, 2017), H^+ receives the electron from Fe^0, forming the active H, which takes part in the deoxidization process, converting NO_3^- to N species (NO_2^-, NH_4^+, or N_2) (Gao, 2003). It's worth noting that more N_2 can be produced, only the appropriate H^+ concentration in solution has been remained. High H^+ concentration may lead to the generation of the undesired NH_4^+, which has to be treated again. Additionally, H^+ can also reduce the accumulation of OH^- generated with the catalytic processes.

$$H^+ + e^- \rightarrow H \qquad (5)$$

$$NO_3^- + H \rightarrow NO_2^- + OH^- \qquad (6)$$

$$NO_2^- + H \rightarrow NO + OH^- \qquad (7)$$

$$NO + NO \rightarrow N_2 + 2O \qquad (8)$$

$$NO + 2H \rightarrow NH + OH^- \qquad (9)$$

$$NH + NH \rightarrow N_2 + 2H \qquad (10)$$

$$NH + 2H + H_2O \rightarrow NH_4^+ + OH^- \qquad (11)$$
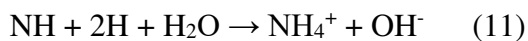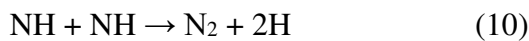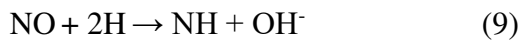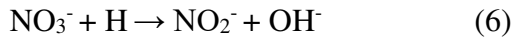
In the catalytic denitrification processes, catalyst composed of the active ingredients and the carrier significantly influences the catalytic performance (Li et al, 2017). The carrier that loads the active ingredients can provide the main reaction sites for the catalytic reaction (Lubphoo et al, 2016).

17

In addition, the physico-chemical properties (pore structure, surface area, mechanical strength, and the chemical components) of the carrier also determines the dispersion degree of the supported active metal particles (Pd, Ag), controls the processes of adsorption, diffusion, reaction, and desorption of the reactants (mainly NO_3^-, NO_2^-) and the products (mainly NH_4^+, N_2) that occurred on the catalyst's surface, which may greatly affect the catalytic reduction of nitrate (He and Li, 2008). Therefore, the materials that possess the porous structure, larger specific surface area, good adsorptive capacity, and stable physico-chemical properties tend to be selected as the carrier of the catalyst.

In addition, the active ingredients can affect the catalytic performance by directly and indirectly participate in the catalytic reaction. Research has found that the active ingredients loaded on the carrier should better comprise of a noble metal (such as Pd or Pt) and an auxiliary element (such as Ag, Cu or In) (Olívia et al. 2011). The bimetallics- Pd and Ag can active the formed H, which will involve the deoxidization process to reduce nitrate. Actually, Ag-H mainly acts with the reactant- NO_3^-, producing NO_2^-. Furthermore, on Pd active sites, the product- NO_2^- can be continued reduce to other N species (NO, NH, N_2, and NH_4^+) (Zhao et al, 2014). The catalytic reaction mechanism is illustrated in Fig. 8.
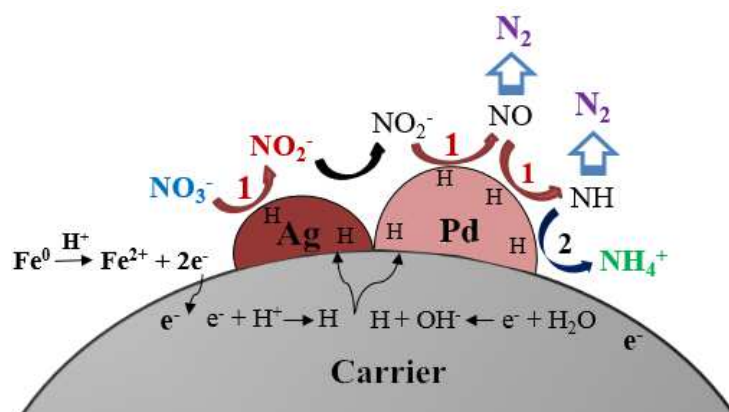

Fig. 8 Catalytic process for nitrate reduction

3.4 Kinetic study

Currently, significant research focuses on the kinetics of catalytic hydrogenation. Rare research on the catalytic process using Fe^0 and bimetallic catalyst to reduce nitrate was conducted. It can be assumed that the zero-order kinetics and first-order equation of Langmuir-Hinshelwood could be employed to describe this process. According to our previous study, the catalytic denitrification process could be better explained by the first order kinetic model (Yun et al. 2018). The kinetic equation could be obtained as the catalyst Pd-Ag/graphene was used: y=247.1x +0.1398, R^2=0.9975.
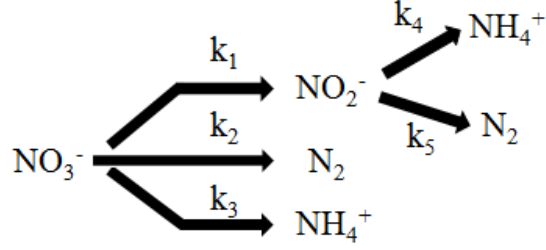
Fig. 9 Catalytic pathway of nitrate reduction

It has been suggested that in the process of catalytic denitrification, the produced intermediates such as NO and NH have been negligible (Lo et al. 2009). The catalytic pathway was proposed, as shown in Fig. 9 (Lubphoo et al. 2016). Based on the first-order equation above, the reaction rates are presented in equations 12-15. A kinetic study on catalytic denitrification with different catalysts was further conducted, as listed in Table 3.

$$\frac{dC_{NO_3^-}}{dt} = -\ (k_1+k_2+k_3)\ C_{NO_3^-} \quad (12)$$

$$\frac{dC_{NO_2^-}}{dt} = k_1\ C_{NO_3^-} - (k_4+k_5)\ C_{NO_2^-} \quad (13)$$

$$\frac{dC_{N_2}}{dt} = -\frac{dC_{NO_3^-}}{dt} - \frac{dC_{NO_2^-}}{dt} = k_2\ C_{NO_3^-} + k_5\ C_{NO_2^-} \quad (14)$$

$$\frac{dC_{NH_4^+}}{dt} = -\frac{dC_{NO_3^-}}{dt} - \frac{dC_{NO_2^-}}{dt} = k_3\ C_{NO_3^-} + k_4\ C_{NO_2^-} \quad (15)$$

Where k_1, k_2, and k_3 are the rate constants for reduction of NO_3^- to NO_2^-, N_2 and NH_4^+, respectively; k_4 and k_5 are the rate constants for reduction of NO_2^- to NH_4^+ and N_2.

Table 8 First-order kinetics of catalytic denitrification with different catalysts

Catalysts	Kinetic equation	R^2	Rate constant 10^2 (min^{-1})					
			k	k_1	k_2	k_3	k_4	k_5
Pd-Ag/SiO$_2$	y=0.0077x+0.9763	0.9972	0.77	0.14	0.43	0.26	0.37	0.53
Pd-Ag/diatomite	y=0.006x+0.9939	0.9976	0.60	0.08	0.32	0.24	0.32	0.42
Pd-Ag/kaolin	y=0.0121x+1.0223	0.9968	1.21	0.23	0.79	0.35	0.47	0.86
Pd-Ag/γ-Al$_2$O$_3$	y=0.0209x+0.8919	0.9977	2.09	0.46	1.12	0.68	0.81	1.24
Pd-Ag/silica gel	y=0.0094x+0.9799	0.9964	0. 94	0.15	0.61	0.29	0.43	0.73
Pd-Ag/graphene	y=0.0414x+0.5349	0.9982	4.14	0.88	2.11	1.21	1.32	2.25

Results indicated that different catalysts performed distinct reaction rates in catalytic denitrification, which can be explained by k value listed in Table 8. According to the calculation, for each catalytic process, the summation of k_1, k_2, k_3 that stands for the overall reaction rate constant

was close to k, which indicates the catalytic denitrification is a stepwise process. Results also indicated that compared to other catalysts, Pd-Ag/graphene showed a higher catalytic rate, which has been proved by the data in Table 2. This may be due to the unique properties of graphene, including the porous structure, active surface area, outstanding electronic properties and promising mechanical and thermal stability (Nurhidayatullaili et al. 2015).

4. Conclusion

In this study, response surface methodology was used to optimize the process of catalytic reduction of nitrate based on the results of single factor experiments. Results indicated that the application of response surface methodology in the condition optimization of catalytic denitrification was proved to be feasible. 71.6% of N_2 Selectivity was obtained under the optimum conditions: 5.1 pH, 127 min reaction time, 3.2 mass ration (Pd: Ag), and 4.2 g/L Fe^0. However, the catons (e.g. K^+, Na^+, Ca^{2+}, Mg^{2+}, and Al^{3+} and anions (Cl^-, SO_4^{2-}, and HCO_3^-) may exist in waterbody performed different influence on catalytic denitrification. Study on reaction mechanism found that the reductant-Fe^0 primarily served as the electron donor in the catalytic process, involving the directional electron transfer from Fe^0 to nitrate, which is then converted into N_2 or less toxic species. The catalytic denitrification can be achieved with the deoxidization processes. Additionally, as the components of the catalyst, active ingredients (e.g. Pd-Ag) and carrier (e.g. graphene) significantly influences the catalytic performance. The catalytic denitrification process could be better explained by the first order kinetic model.

References

Choi E, Park K, Lee H, Cho M, Ahn S (2013) Formic acid as an alternative reducing agent for the catalytic nitrate reduction in aqueous media. Journal of Environmental Sciences 25:1696-1702

Cui B, Zhang F, Xu S, Liu S (2008) Study on Catalytic reduction of removal nitrate in drinking water. Applied Chemical Industry 7:1081-1085

Dadras FS, Gharanjig K, Raissi S (2014) Optimising by response surface methodology the dyeing of polyester with a liposome-encapsulated disperse dye. Coloration Technology 130(2): 86-92

Deganello F, Liotta LF, Macaluso A, Venezia AM, Deganello G (2000) Catalytic reduction of nitrates and nitrites in water solution on pumice-supported Pd-Cu catalysts. Appl. Catal. B: Environ 24:265-273

Gao W, Guan N, Chen J, Guan X, Jin R, Zhuang F (2003) Titania support Pd-Cu bimetallic catalyst for the reduction of nitrate in drinking water. Applied Catalysis B: Environmental 46:341-351

Haddar W, Elksibi I, Meksi N, Mhenni MF (2014) Valorization of the leaves of fennel (Foeniculum vulgare) as natural dyes fixed on modified cotton: a dyeing process optimization based on a response surface methodology. Ind. Crop. Prod 52:588-596

Hao S, Zhang H (2017) High Catalytic performance of nitrate reduction by synergistic effect of zero-valent iron (Fe^0) and bimetallic composite carrier catalyst. Journal of Cleaner Production 167: 192-200

He Hong, Li Junhua. Environmental catalysis: mechanism and application. Beijing Science Press. 2008

Imran MA, Awais HT (2016) Modelling the properties of one-step pigment-dyed and finished polyester/cotton fabrics using response surface methodology. Coloration Technology 132(5): 414-420

Jasper JT, Jones ZL, Sharp JO, Sedlak DL (2014) Nitrate removal in shallow, open-water treatment wetlands. Environ. Sci. Technol 48:11512-11520

Jung S, Bae S, Lee W (2014) Development of Pd-Cu/Hematite Catalyst for Selective Nitrate Reduction. Environ. Sci. Technol 48:9651-9658

Kabdasli I, Coskun B (2015) Evaluation of the optimal operation conditions using response surface methodology for the aqueous DMP solution by electrocoagulation. Global Nest J 17(2):248-256

Khalil AME, Eljamal O, Jribi S, Matsunaga N (2016) Promoting nitrate reduction kinetics by nanoscale zero valent iron in water via copper salt addition. Chemical Engineering Journal 287: 367-380

Li PJ, Lin KR, Fang ZQ, Wang KM (2017) Enhanced nitrate removal by novel bimetallic Fe/Ni nanoparticles supported on biochar. Journal of Cleaner Production 151:21-33

Lo SL, Liou YH, Lin CJ, Weng SC, Ou HH (2009) Selective decomposition of aqueous nitrate into nitrogen using iron deposited bimetals. Environ. Sci. Technol 43: 2482-2488

Lubphoo Y, Chyan JM, Grisdanurak N, Liao CH (2016) Influence of Pd-Cu on nanoscale zero-valent iron supported for selective reduction of nitrate. Journal of the Taiwan Institute of Chemical Engineers 59: 285-294

Mcadam EJ, Judd SJ (2006) A review of membrane bioreactor potential for nitrate removal from drinking water. Desalination 196:135-148

Min SK, Sang HC, Chun JY, Myung SL, Hyoung C, Dae WL, Kwan YL (2013) Catalytic reduction of nitrate in water over Pd–Cu/TiO_2 catalyst: effect of the strong metal-support interaction (SMSI) on the catalytic activity. Appl. Catal. B: Environ 142-143: 354–361

Nathany A, Mehra N, Patwardhan AV (2014) Optimisation of concentration of ingredients for

simultaneous dyeing and finishing using response surface methodology. Journal of the Textile Institute105(11): 1146-1159

Nurhidayatullaili MJ, Samira B (2015) Graphene supported heterogeneous catalysts: An overview. International Journal of Hydrogen Energy 4:948-979

Olívia SGP, Soares José JM, Órfão A, Manuel FR, Pereira (2011) Nitrate reduction in water catalysed by Pd-Cu on different supports. Desalination 279:367–374.

Ryu A, Jeong SW, Jang A, Choi H (2011) Reduction of highly concentrated nitrate using nanoscale zero-valent iron: effects of aggregation and catalyst on reactivity. Appl. Catal. B: Environ 105: 128-135

Shen J, Zhu Z, Jin W, Wang C, Jiang Y (2016) Comparison of orthogonal design and response surface method for extraction of polyphenols from pomegranate peel by microwave method. Journal of Zhejiang Shuren University 16(4):31-35

Schlicker O, Ebert M, Fruth M, Weidner M, Wüst W, Dahmke A (2000) Degradation of TCE with iron: The role of competing chromate and nitrate reduction. GROUND WATER 38(3): 403-409

Soares MIM (2000) Biological denitrification of groundwater. Water Air Soil Poll 123:183-193

Vorlop KD, Tacke T (1989) 1st steps towards noble-metal catalyzed removal of nitrate and nitrite from drinking water. Chem. Ing. Tech 61:836-837

Ye Z, Wang W, Yuan Q, Ye H, Sun Y, Zhang H, Zeng X (2016) Box–Behnken design for extraction optimization, characterization and in vitro antioxidant activity of Cicer arietinum L. hull polysaccharides. Carbohydrate polymers 147:354-364.

Yu Chengbing, Tao Kaixin, Hou Qi-ao, Wu Congjie (2018) Optimization of wet-steam dyeing technology of cotton knitting fabric by response surface and central composite design. Advanced Textile Technology 1-6

Yun YP, Li ZF, Chen YH, Saino M, Cheng SK, Zheng L (2016) Reduction of Nitrate in Secondary Effluent of Wastewater Treatment Plants by Fe^0 Reductant and Pd-Cu/Graphene Catalyst. Water Air and Soil Pollution 227(4):1-10

Yun YP, Li ZF, Chen YH, Saino M, Cheng S, Zheng L (2018) Elimination of nitrate in secondary effluent of wastewater treatment plants by Fe^0 and Pd-Cu/diatomite. Water reuse and desalination 1:29-37

Zhang Y (2003) Catalytic reduction of nitrates from groundwater. Zhejiang University.

Zhao W, Zhu X, Wang Y, Ai Z, Zhao D (2014) Catalytic reduction of aqueous nitrate by metal supported catalysts on Al particles. Chemical Engineering Journal. 254:410-417
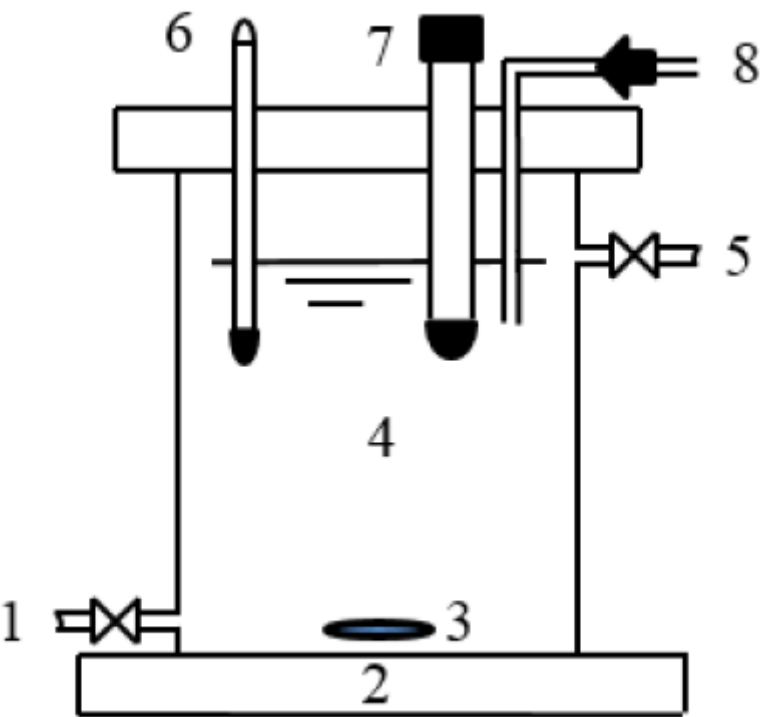
Figures

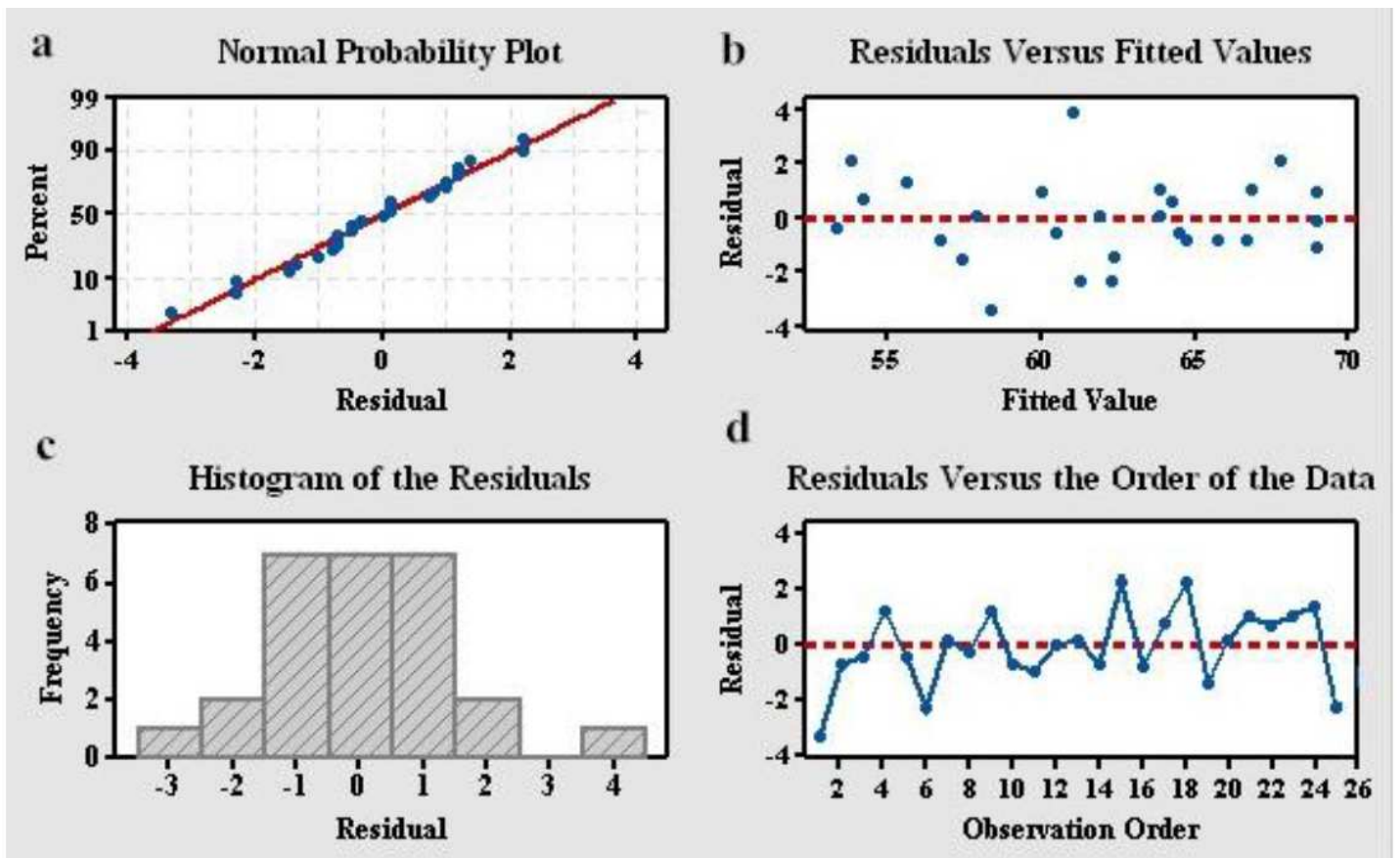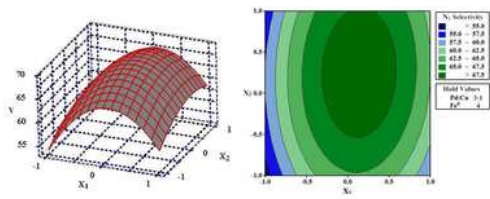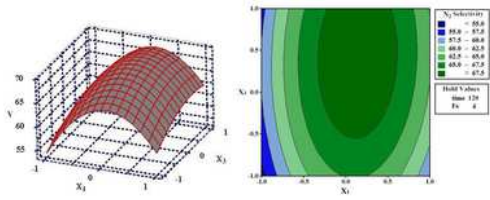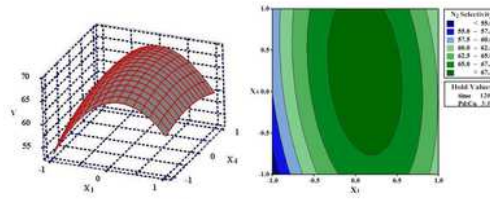**Figure 1**

Schematic of the reactor
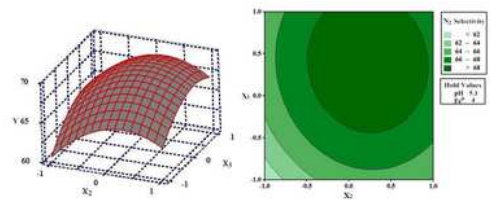
Figure 2

Residual plots for N2 selectivity

a Response surface (Left) and Contour plots (Right) of X_1 and X_2 on N_2 selectivity
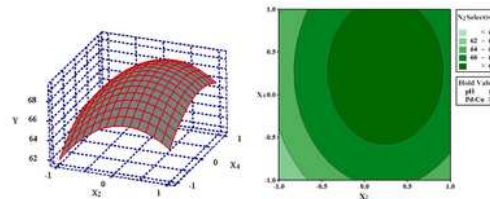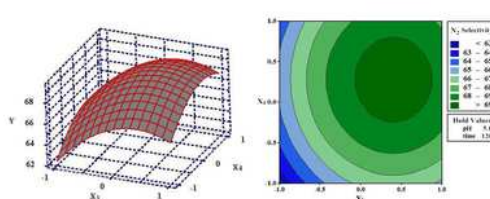
b Response surface (Left) and Contour plots (Right) of X_1 and X_3 on N_2 selectivity

c Response surface (Left) and Contour plots (Right) of X_1 and X_4 on N_2 selectivity

d Response surface (Left) and Contour plots (Right) of X_2 and X_3 on N_2 selectivity

e Response surface (Left) and Contour plots (Right) of X_2 and X_4 on N_2 selectivity

f Response surface (Left) and Contour plots (Right) of X_3 and X_4 on N_2 selectivity

Figure 3

Response surface and Contour plots between two factors
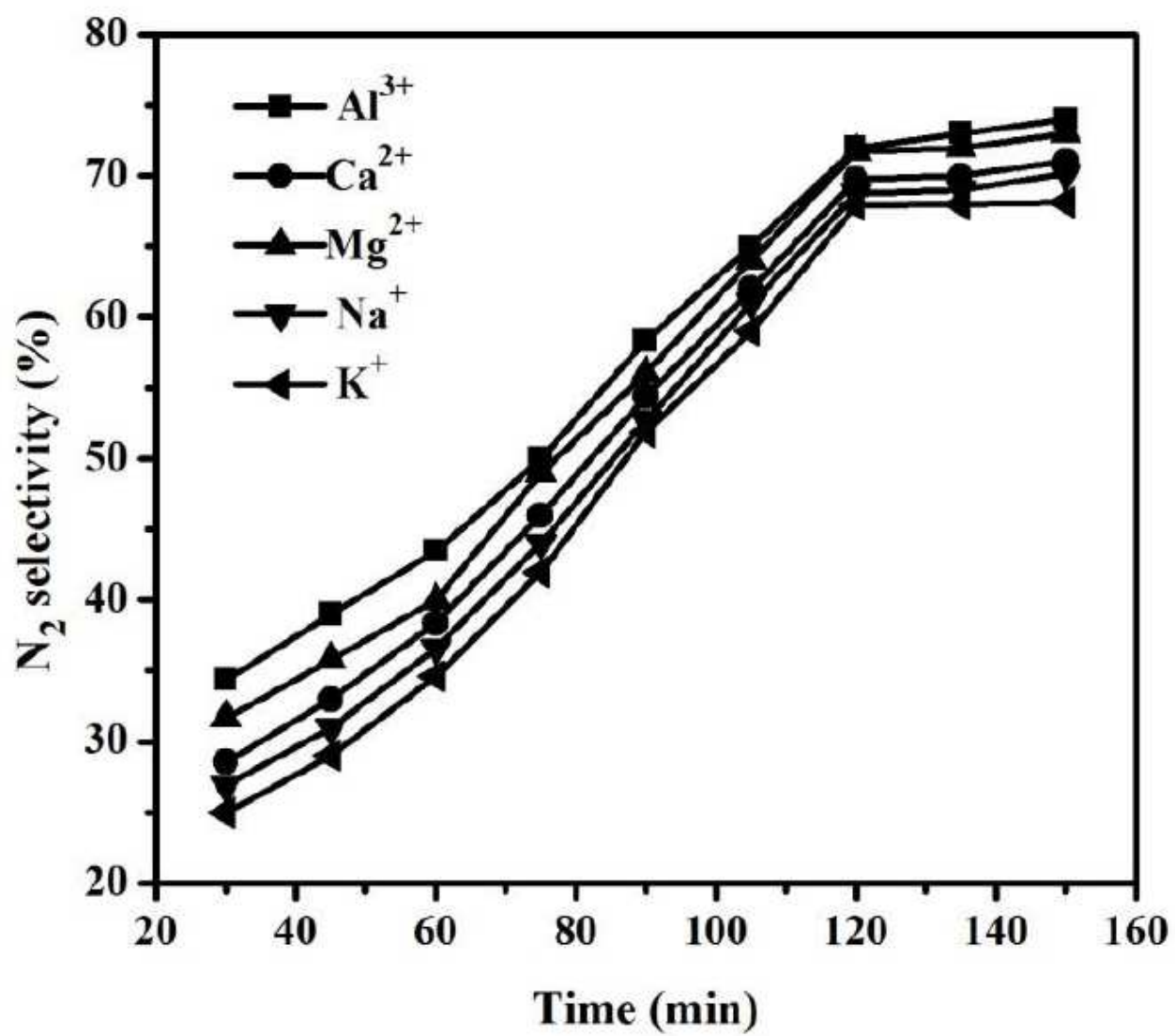
Figure 4

Catalytic performances with different cations in solution (pH 5.1, 127 min, 4.2 g/L Fe0, 4 g/L Pd-Ag/graphene, Pd:Ag=3:1, Pd: 5 wt%)
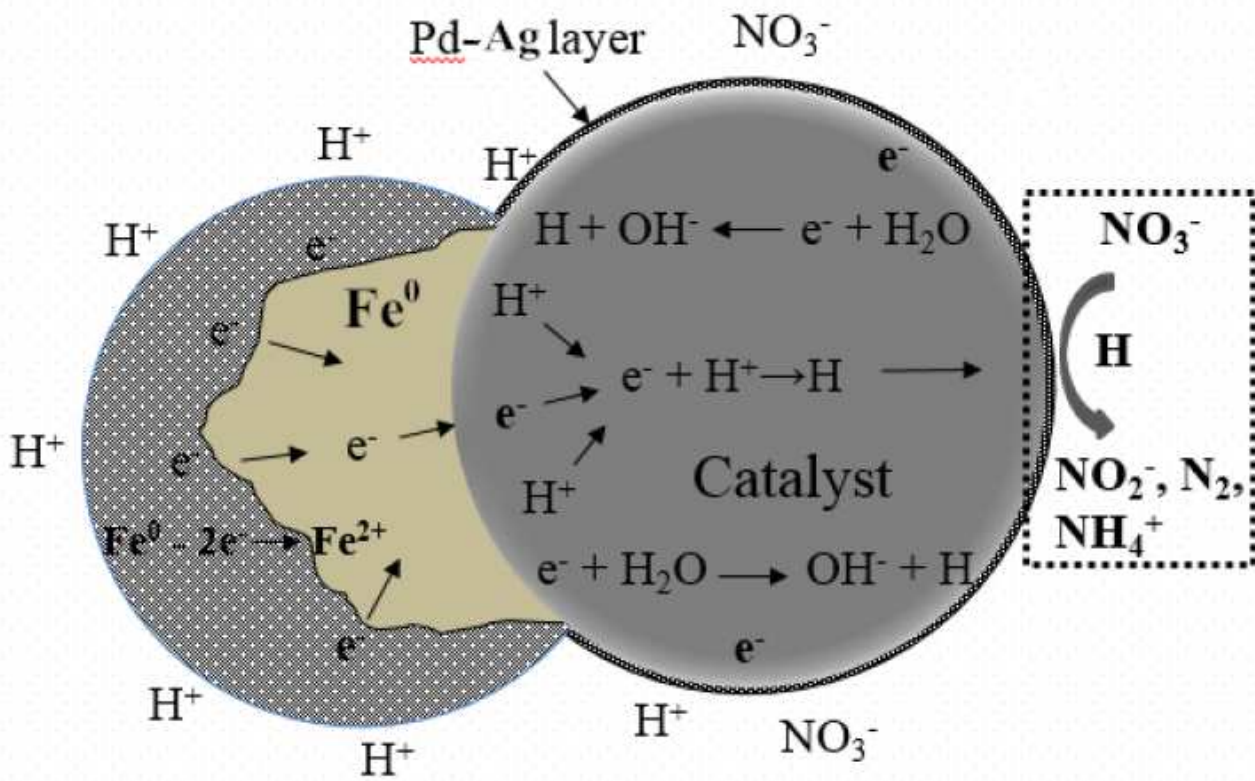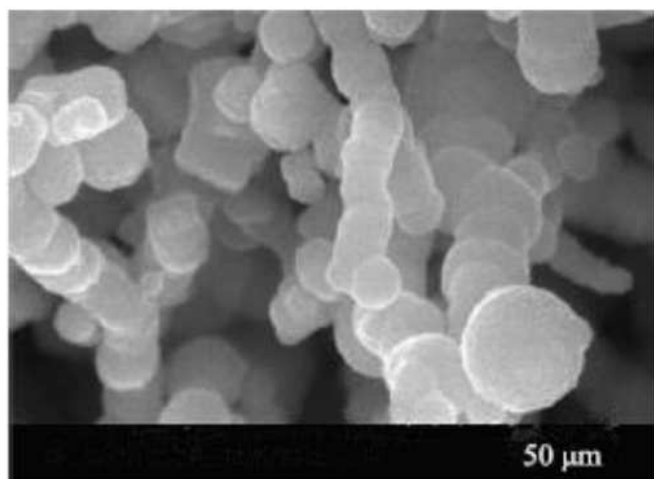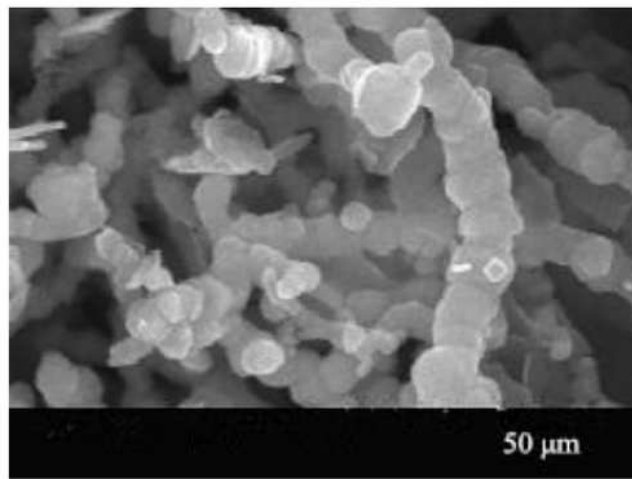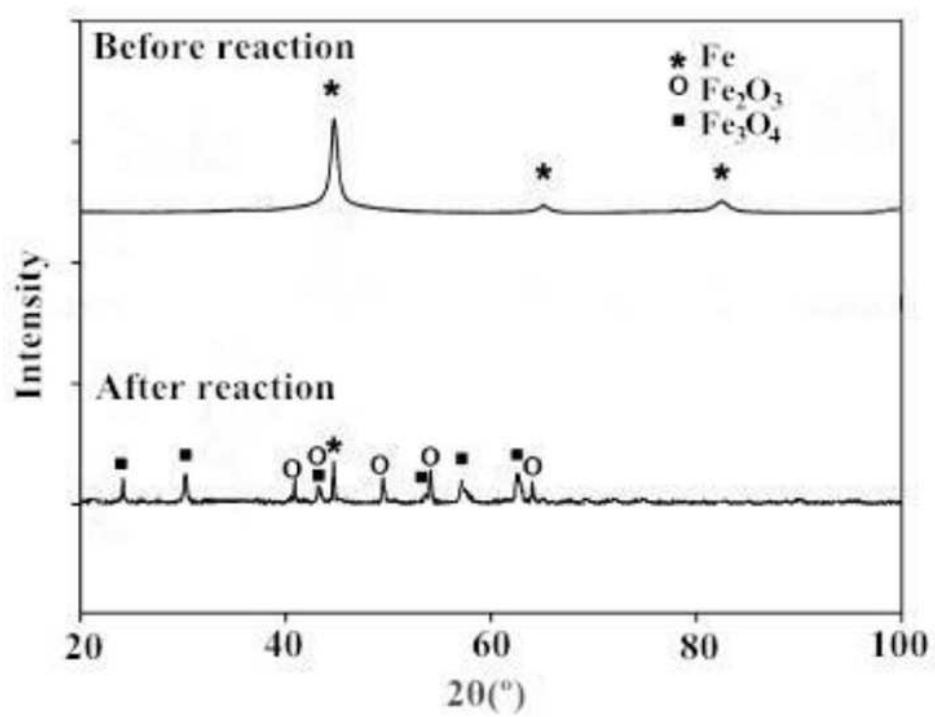
Figure 6

Role of Fe0 in catalytic process

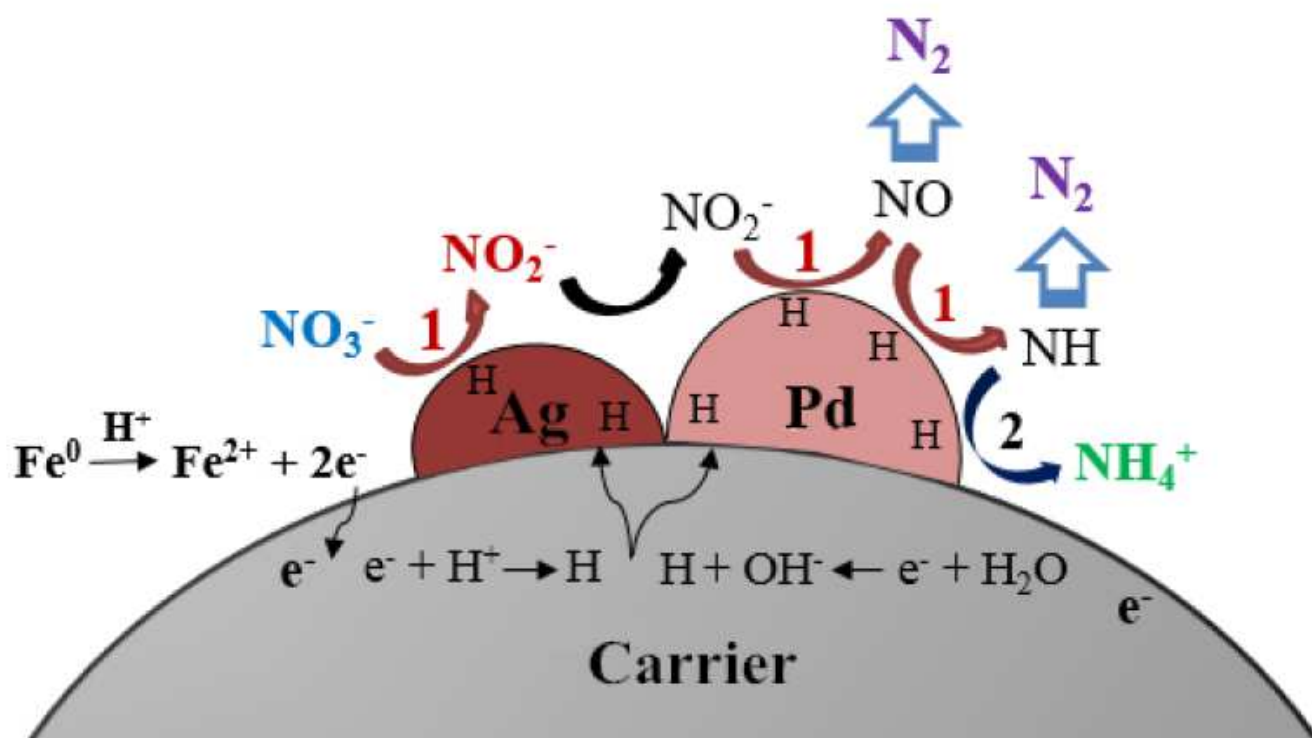Figure 7

SEM images and XRD patterns of Fe0

Figure 8

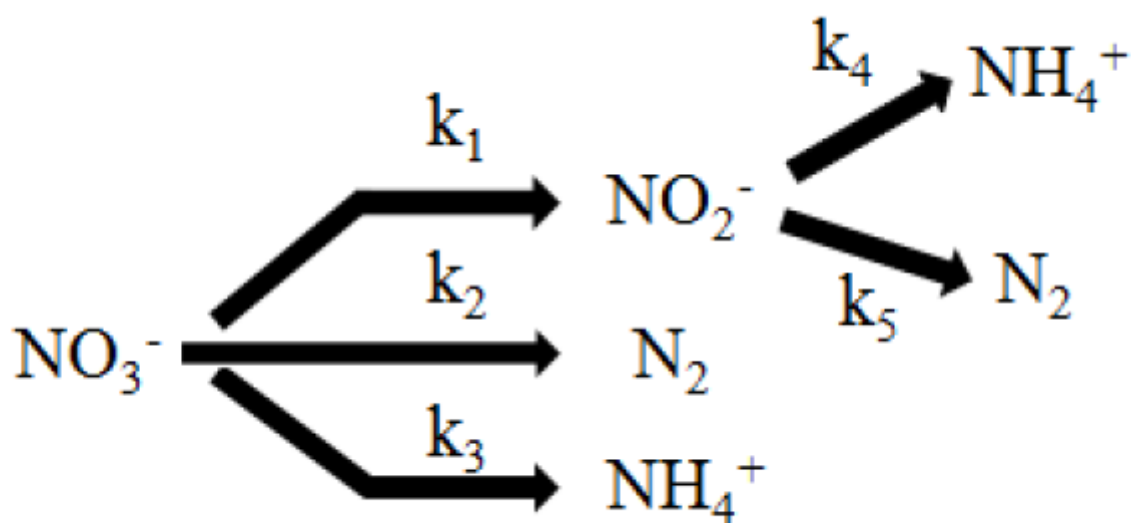Catalytic process for nitrate reduction

Figure 9

Catalytic pathway of nitrate reduction

Supplementary Files

This is a list of supplementary files associated with this preprint. Click to download.

- GraphicalAbstract.docx